Monthly Notices of the ROYAL ASTRONOMICAL SOCIETY

MNRAS **518,** 4038–4044 (2023) https://doi.org/10.1093/mnras/stac3343
Advance Access publication 2022 November 17

HD 16424: A new weak *G*-band star with high Li abundance

N. Holanda [1]★ N. A. Drake[1,2,3] and C. B. Pereira[1]

[1]*Observatório Nacional, Rua General José Cristino 77, CEP 20921-400, São Cristóvão, Rio de Janeiro, RJ, Brazil*
[2]*Laboratory of Observational Astrophysics, Saint Petersburg State University, Universitetski pr. 28, 198504 Saint Petersburg, Russia*
[3]*Laboratório Nacional de Astrofísica/MCTI, Rua dos Estados Unidos 154, Bairro das Nações, 37504-364 Itajubá, Brazil*

Accepted 2022 November 10. Received 2022 November 3; in original form 2022 September 6

ABSTRACT

The origin of the so-called weak *G*-band stars constitutes an unsolved problem in stellar astrophysics. In this context, we present a detailed abundance analysis of a new weak *G*-band star, HD 16424, which stands out with a very low $^{12}C/^{13}C$ ratio and Li and Na overabundance. Our work is based on the high-resolution échelle spectrum ($R \approx 48\,000$) and includes photometric and astrometric data from the literature. The analysis adopted in this work is performed under local thermodynamic equilibrium (LTE) approximation; we determine the atmospheric parameters ($T_{\rm eff}$, log g, [Fe/H], and ξ), abundances for proton-capture elements (C, N, O, Li), *s*-process elements (Y, Zr, La), and mixing tracers such as the $^{12}C/^{13}C$ isotopic ratio and sodium abundance, following by NLTE corrections applied to Li, O, and Na abundances. Our results show ^{12}C deficiency ([C/Fe] $= -0.57$) and N enrichment ([N/Fe] $= +0.97$), that is typical for weak *G*-band stars. Also, we notice a carbon isotopic ratio characteristic of the CN-cycle equilibrium ($\langle ^{12}C/^{13}C \rangle = 4.0$) and high lithium-7 abundance (log $\varepsilon(\mathrm{Li})_{\rm NLTE} = 2.85$). In addition, this study shows a low projected rotational velocity ($v \sin i = 2.0\,\mathrm{km\,s^{-1}}$) and low mass ($1.61\,M_\odot$) of HD 16424, which distinguishes this star from the intermediate-mass objects found in this class of peculiar objects.

Key words: stars: abundances – stars: chemically peculiar – stars: fundamental parameters – stars: individual: HD 16424.

1 INTRODUCTION

The weak *G*-band stars (hereafter WGBs) or weak CH stars are intriguing objects: as the main characteristic, this class of stars presents weak CH molecular lines in the Fraunhofer *G*-band ($A^2\Delta - X^2\Pi$ system at 4300 Å), which is caused by deficiency of the carbon-12 (Rao 1978). These peculiar stars are so rare that their share among the G-K giants in the Bright Star Catalogue ($83^\circ < \delta < +6^\circ$) is less than 0.3 per cent (Bidelman & MacConnell 1973; Palacios et al. 2016). Also, the WGB stars are notable for presenting nitrogen overabundance and sometimes sodium and lithium enrichment (Lambert & Sawyer 1984; Palacios et al. 2012; Adamczak & Lambert 2013). The first report about WGB stars was done by Bidelman (1951), who underlines their main feature. However, despite an ancient report about the first WGB star, HR 885, the origin of this peculiar giant star (its formation mechanism) remains an open question in the literature.

In the colour–magnitude diagram (CMD), the WGBs are at the base or ascension to the red giant branch (RGB) or in the red clump (RC) stage. For instance, Tsvetkova et al. (2017) point out that 37 Com – a well-known object – is located in the Hertzsprung gap, but Bond (2019) alerted for dubious regions in the evolutionary stage of many WGBs (Gap, RGB, and RC). Regarding their masses, many studies show that WGB stars are typically intermediate-mass stars, with values in the range of 2.0–5.0 $M_\odot$ (Palacios et al. 2012, 2016; Adamczak & Lambert 2013; Bond 2019). Therefore, low-mass stars are uncommon in this class.

There are hypotheses in the literature to explain the formation of WGB stars. The rotationally induced mixing is a possible cause for the WGB phenomenon: this scenario considers rapidly rotating intermediate-mass main sequence stars as progenitors. However, there is a strong dependence on most parameters; otherwise, the WGB phenomenon would be frequent and not be an odd phenomenon for G–K giants (Adamczak & Lambert 2013). Alternatively, Palacios et al. (2016) made suppositions about whether these stars been born polluted or polluted shortly after their birth by massive objects. Bond (2019) supported another scenario based on binary mass transfer and mergers: he argues about the distances from the Galactic plane observed to the WGB stars, which seem systematically larger compared to the ordinary red giant stars. This possibility was (first) raised by Izzard et al. (2018), who explored the binary population in the thick disc which is eventually more massive than should be given by their age ($> 1.3\,M_\odot$).

HD 16424 is a bright target neglected so far. We are providing its report as a WGB star and carry out a comprehensive chemical analysis for this odd object. Our methodology to obtain the atmospheric parameters and abundances is described in Section 2. Also, we take from the literature a set of additional data to check and expand the results obtained from the spectroscopic analysis. Then, a discussion of the results is presented in Section 3. Lastly, some conclusions and remarks are provided in Section 4.

2 METHODOLOGY

2.1 Observations

The spectrum of HD 16424 was obtained on 2007 August 28, with the Échelle spectrograph Fiber-fed Extended Range Optical

★ E-mail: nacizoholanda@on.br

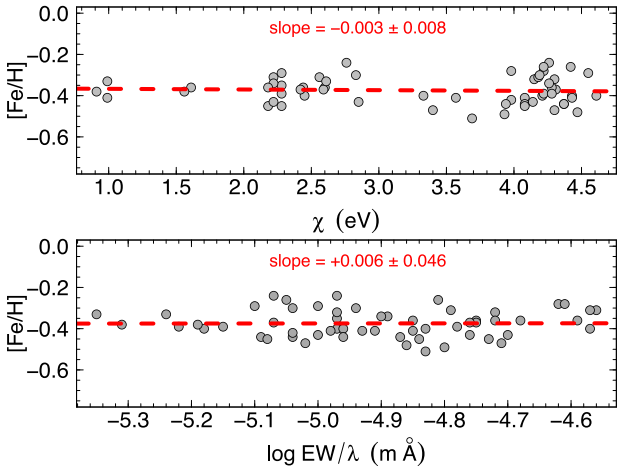

Figure 1. Iron abundance versus excitation potential (top) and versus reduced equivalent width (bottom). The red dashed lines represent the linear regression with the angular coefficient close to zero.

Spectrograph (FEROS; Kaufer et al. 1999) attached to the 2.2 m Max Planck Gesellschaft/European Southern Observatory (ESO) Telescope, Chile. FEROS spectrograph can provide spectroscopic data in a wide spectral range (3700 Å – 9000 Å), having a spectral resolution (R≈48 000) that is sufficient to resolve individual absorption atomic lines. Also, our spectrum has a high signal-to-noise ratio (S/N = 160 at 6000 Å) obtained with an exposure time of 1500 s; this is suitable for our methodology which is based on the measurements of equivalent widths of some selected absorption lines and the use of the spectral synthesis technique.

2.2 Atmospheric and physical parameters

The atmospheric parameters were obtained in the same way as in Holanda et al. (2022): first, we measure the equivalent widths of iron lines using the IRAF (Tody 1986) and the routine *splot*. The line list was taken from Lambert et al. (1996). We obtained measurements from intervals of 4900 Å to 7200 Å following the condition $20 < \mathrm{EW} < 160$ mÅ for a Gaussian adjustment – a total of 58 Fe I and 16 Fe II lines. The unblended iron lines were used to constrain the best stellar atmosphere parameters with the help of routine *abfind* in the code MOOG (2013 version; Sneden 1973) and the atmosphere Kurucz's models (Kurucz 1993), under the LTE assumption.

We assumed the excitation equilibrium to obtain the effective temperature, which is verified through no trend in the correlation coefficients between iron abundances derived from Fe I lines and the lower excitation potential (χ). Also, the microturbulent velocity (ξ) was found by constraining the abundance determined from individual Fe I lines, until they also show no dependence on reduced equivalent width, log EW/λ. We can check both conditions with plots in Fig. 1. Furthermore, the value of surface gravity (log g) is determined by imposing the ionization equilibrium. This condition is satisfied by reaching practically equal abundances for Fe I and Fe II: we obtained log ε(Fe I) = 7.12 ±0.07 and log ε(Fe I) = 7.13 ± 0.07.

The error in $T_{\rm eff}$ was calculated from the uncertainty in the slope of relation Fe I versus the χ, while the error in ξ was obtained from the uncertainty in the slope of Fe I abundance versus log EW/λ. For the surface gravity, the error is estimated by changing the log g value until the difference in the average abundances of Fe I and Fe II equals the standard deviation of the mean [Fe I/H]. The atmospheric parameters with their respective uncertainties are shown in Table 1.

Table 1. Derived stellar parameters of HD 16424. References: Houk & Smith-Moore (1988), H1988; Høg et al. (2000), H2000; Pickles & Depagne (2010), PD2010; Cutri et al. (2013), C2013.

Parameter	Value	Reference
RA (J2000)	02 37 47.368	–
DEC (J2000)	−14 36 08.747	–
V (mag)	9.472 ± 0.030	H2000
K_s (mag)	7.113 ± 0.018	C2013
W_1 (mag)	6.995 ± 0.050	C2013
W_4 (mag)	6.958 ± 0.073	C2013
Spectral type	G8 III/IV	H1988
Spectral type	K0 III	PD2010
V_r (km s^{-1})	−29.83 ± 0.21	G2018
V_r (km s^{-1})	−29.85 ± 0.29	This Work
π (mas)	1.3905 ± 0.0479	G2018
pmRA (mas yr^{-1})	+5.397	G2018
pmDE (mas yr^{-1})	−12.318	G2018
$R_{\rm GC}$ (kpc)	8.32	This Work
$U_{\rm LSR}$ (km s^{-1})	−36.33	This Work
$V_{\rm LSR}$ (km s^{-1})	−27.36	This Work
$W_{\rm LSR}$ (km s^{-1})	−30.14	This Work
$T_{\rm eff}$ (K)	4850 ± 40	This Work
$T_{\rm eff,\,(V\text{-}K)}$ (K)	4878 ± 40	This Work
log g (cm s^{-2})	2.60 ± 0.10	This Work
log $g_{\rm phot}$ (cm s^{-2})	2.61 ± 0.18	This Work
ξ (km s^{-1})	1.51 ± 0.04	This Work
[Fe I/H] (dex)	−0.38 ± 0.07	This Work
[Fe II/H] (dex)	−0.37 ± 0.07	This Work
v sin i (km s^{-1})	2.0 ± 0.3	This Work
M ($M_\odot$)	1.61 ± 0.26	This Work
R ($R_\odot$)	12.95 ± 0.61	This Work
log L ($L_\odot$)	1.74 ± 0.10	This Work
t (Gyr)	1.95 ± 0.91	This Work

According to the PARSEC evolutionary tracks (PAdova and TRieste Stellar Evolution Code; Bressan et al. 2012) and a Bayesian estimation method (da Silva et al. 2006), HD 16424 has a mass of $M = 1.61 \pm 0.26\,M_\odot$ and age of $t = 1.950 \pm 0.914$ Gyr. This estimation has been made through PARAM,[1] a helpful tool to estimate the basic intrinsic parameters of stars given by their photometric and spectroscopic data. In addition, from the PARAM outputs, we obtain the luminosity of the star through the formula

$$\log\left(\frac{L}{L_\odot}\right) = \log\left(\frac{M}{M_\odot}\right) - 4\log\left(\frac{T_{\rm eff,\odot}}{T_{\rm eff}}\right) - \log\left(\frac{g}{g_\odot}\right),$$

where the solar values adopted are log $g_\odot$ = 4.44 dex and $T_{\rm eff}$ = 5777 K. In addition, we have used the polynomials by Alonso, Arribas & Martínez-Roger (1999) for fitting effective temperature as a function of $(V - K)$ colour and [Fe/H] to obtain photometric temperature feedback, of $T_{\rm eff,\,(V\text{–}K)}$ = 4878 ± 40 K; which is necessary for photometric gravity. So we applied the well-known expression to find log $g_{\rm phot}$:

$$\log g_{\rm phot} = \log\left(\frac{M}{M_\odot}\right) + 0.4(K - A_K + BC_K) + 4\log T_{\rm eff,(V-K)} - 2\log\left(\frac{1}{\pi}\right) - 16.5.$$

[1] Available on http://stev.oapd.inaf.it/cgi-bin/param_1.3

For K, A_K, and BC_K meaning, respectively, the apparent magnitude, interstellar absorption, and bolometric correction in the K band. The surface gravity, mass, temperature, and parallax of the star are, respectively, log $g_{\rm phot}$, M, $T_{\rm eff,\,(V-K)}$, and π. We obtained $A_V = 0.139$ from McDonald, Zijlstra & Watson (2017), but the relation to finding out A_K and BC_K was estimated according to Bessell, Castelli & Plez (1998). Finally, we obtained log $g_{\rm phot} = 2.61 \pm 0.18$, that is in good agreement with the value determined spectroscopically of 2.60. Furthermore, the spectroscopic and photometric temperature results found here are in good agreement with those found in the literature: Ammons et al. (2006), 4795 K; Gontcharov (2008), 4900 K; McDonald et al. (2017), 4841 K; Tonry et al. (2018), 4893 K; and Bai et al. (2019), 4926 K.

To complement the spectroscopy analysis, we have combined photometric data from The Tycho-2 Catalogue (Høg et al. 2000) and astrometric data from the ESA Gaia Mission (Gaia Collaboration 2018, hereafter G2018). We have calculated the Galactic space velocity for HD 16424 considering proper motion and parallax taken from G2018. The radial velocity was obtained by measuring the Doppler shifts of 4 Fe I absorption lines (5584.8 Å, 6027.1 Å, 6608.0 Å, and 7130.9 Å) and we found a value of -29.85 km s^{-1}, that is in excellent concordance with the V_r value from G2018 ($\Delta V_r = 0.02$ km s^{-1}). The procedure to obtain the space velocities follows the standard procedure given by Johnson & Soderblom (1987) with exception of U which we considered positive towards the Galactic anticentre. Finally, the velocities were corrected to the local standard of rest (LSR) assuming a solar motion of $(U, V, W)_\odot = (-8.5, 13.38, 6.49)$ km s^{-1} given by Coşkunoğlu et al. (2011).

The projected rotational velocity ($v \sin i$, where v and i represent the rotational velocity at the star equator and the inclination of the stellar rotation axis to the line of sight) was estimated as described by Holanda et al. (2021): by using a spectral synthesis of 5 absorption lines (6151.6 Å, 6219.2 Å, 6232.7 Å, 6246.6 Å, and 6252.5 Å; Gray 1989) using the driving SYNTH from code MOOG, we fixed macroturbulent velocity at 3.0 km s^{-1} (as in Fekel 1997 for G–K giants) and considered the instrumental broadening of the FEROS spectral resolution (FWHM $\approx$ 0.13 Å), while $v \sin i$ was obtained using an iterative procedure until we find the smallest difference between the synthetic and observed spectra. So, it is found a very low rotational velocity result, which causes small distortion in line profiles. The standard deviation from the mean V_r and $v \sin i$ values. Basic parameters are presented in Table 1.

2.3 Abundances

We have employed the spectral synthesis technique to determine abundances of lithium, carbon, and nitrogen. The equivalent width measurements were employed to obtain the abundances of O, Na, Y, Zr, and La. These species were chosen based on main 'anomalies' observed in the phenomenon of weak G-band stars so far reported in the literature.

First, the lithium abundance was obtained using the resonance doublet at λ 6708 Å. The input archive with wavelengths and gf-values for the lithium lines was taken from Smith, Lambert & Nissen (1998), Hobbs, Thorburn & Rebull (1999), and The Vienna Atomic Line Database (VALD; Kupka et al. 1999). Fig. 2 (bottom) shows the spectral synthesis around the region at 6708 Å where we obtained the lithium abundance of log $\varepsilon(\rm Li)_{\rm LTE} = +3.03$ dex. Furthermore, we used the $^{12,\,13}$CH lines of the $A^2\Delta - X^2\Pi$ system at 4363 Å for the synthesis procedure and carbon abundance

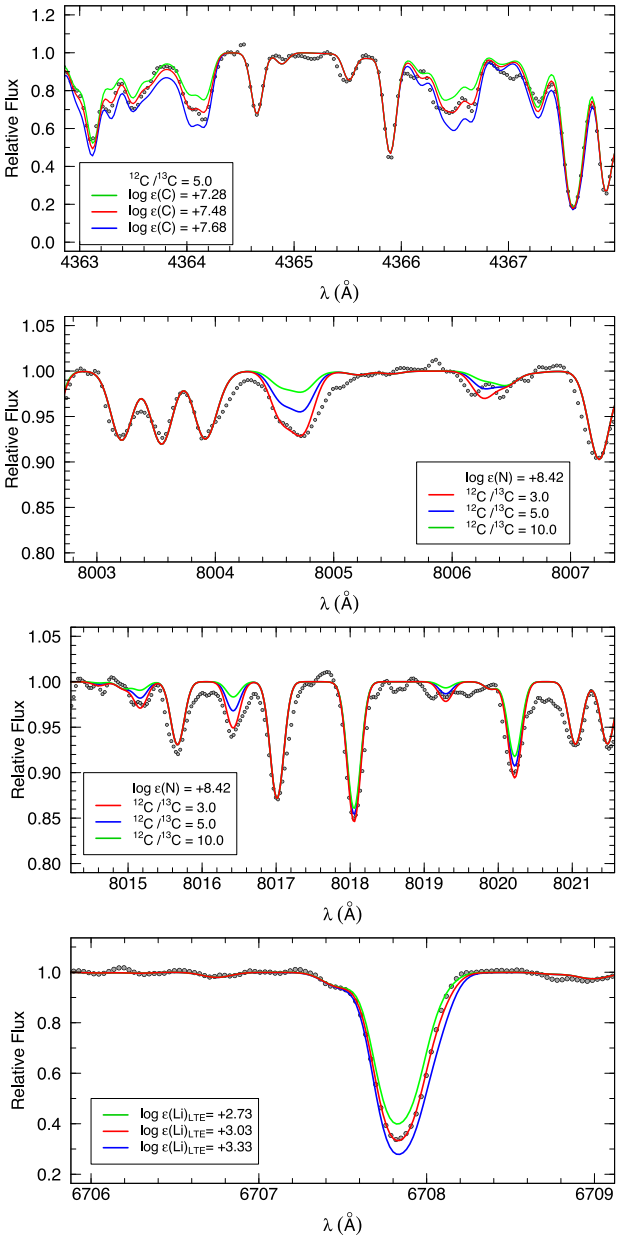

Figure 2. Best fits obtained between the synthetic and the observed FEROS spectra of HD 16424 around CH band (upper), CN band (middle), and $^{6,\,7}$Li lines (bottom).

determination: for this region our spectral synthesis provide the result of ^{12}C/^{13}C = 5.0 and log ε(C) = +7.48, simultaneously. The abundance of nitrogen was obtained by the $^{12,\,13}$CN lines $A^2\Pi - X^2\Sigma$ in the 8002–8020 Å wavelength range, as well as ^{12}C/^{13}C in six different regions in this range. This procedure requires a C abundance fixed (first step) when we found the first N abundance result, then the procedure was repeated again and the derived CNO abundances are reviewed. Finally, we found ^{12}C/^{13}C = 3.0 and log ε(N) = +8.42, therefore a mean value of $\langle^{12}\rm C/^{13}C\rangle = 4.0$ takes into account CH and CN syntheses. Fig. 2 (top and middle) shows spectral synthesis for CH and CN regions used to obtain the abundances for carbon and nitrogen and carbon ^{12}C/^{13}C ratio. Line lists for the abovementioned regions are described by Drake & Pereira (2008).

Table 2. Derived abundances for HD 16424. The last column shows the solar abundances by Asplund et al. (2009).

Species	[X/Fe]	log ε(X)$_{\rm LTE}$	log ε(X)$_{\rm NLTE}$	log ε(X)$_{\odot}$
Li I	–	3.03	2.85	1.05
C (CH)	−0.57	7.48	–	8.43
N (CN)	+0.97	8.42	–	7.83
O I	+0.34	8.81	8.65	8.69
Na I	+0.35	6.31	6.21	6.24
Fe I	–	7.12	–	7.50
Y II	−0.10	1.73	–	2.21
Zr I	−0.03	2.17	–	2.58
La II	+0.07	0.79	–	1.10

Unfortunately, the oxygen abundance based on the forbidden line at 6300 Å is unfeasible because of the contamination by telluric O_2 line. Knowing this difficulty, oxygen abundance was inferred from the analysis of the 7771–7775 Å O I triplet with the *gf*-values taken from the National Institute of Standards and Technology[2] (NIST; Wiese, Smith & Miles 1969). The equivalent width technique was implemented in this case, with EW values of 39, 34, and 27 mÅ for the oxygen lines at 7770 Å.

The effects of the non-local thermodynamical equilibrium for the oxygen triplet at 7771 Å, 7774 Å, and 7775 Å and for the lithium line at 6708 Å are significant and need to be taken into account in order to obtain a correct abundance value. To make these corrections, we have adopted the grids by Ramírez, Allende Prieto & Lambert (2007) for oxygen and Lind, Asplund & Barklem (2009) for lithium. In general, NLTE corrections for oxygen triplet have a negative sign and in this case, we found a mean value of $\Delta \log \varepsilon(\mathrm{O}) = -0.16$ dex. For lithium, the sign and the strength of the NLTE corrections vary from author to author: we found a difference of −0.18 after NLTE correction.[3]

For *s*-process elements, we determined abundance for singly ionized yttrium taking into account atomic parameters from Sneden et al. (1996), Van Winckel & Reyniers (2000), and Reddy et al. (2003). Also, the abundance value for neutral zirconium was obtained with parameters taken from Antipova et al. (2005) and Smith et al. (1996). To determine the lanthanum abundance, we used the driver *blends* in MOOG to find the abundance value, which required EW of a complex spectral feature. Atomic parameters were taken from Lawler, Bonvallet & Sneden (2001) and Roriz et al. (2021) to construct our line list. In this process were measured four lines of Y II (4883.7 Å, 5200.4 Å, 5289.8 Å, and 5402.8 Å), six lines of Zr I (4772.3 Å, 4815.6 Å, 5879.8 Å, 6127.5 Å, 6134.6 Å, and 6143.2 Å), and three lines of La II (5303.5 Å, 6320.4 Å, and 6774.3 Å). Finally, a mean abundance of the *s*-process elements was calculated, $[s/\mathrm{Fe}] = -0.02 \pm 0.08$.

The sodium abundance was obtained by measuring the equivalent widths of the Na I lines at 6154 Å and 6161 Å, where *gf*-values were taken from Reddy et al. (2003). But it is known that these sodium lines also suffer from non-local thermodynamic equilibrium (NLTE) effects which can lead us to a misinterpretation of the sodium abundances; in this sense, we corrected the abundance given by each line according to the tables given in Lind et al. (2011). After that, it is observed an abundance difference of −0.10 with respect to the one obtained under the LTE assumption. The final abundances for HD 16424 are given in Table 2.

[2]Available on https://physics.nist.gov
[3]We used a tool available on http://inspect-stars.com

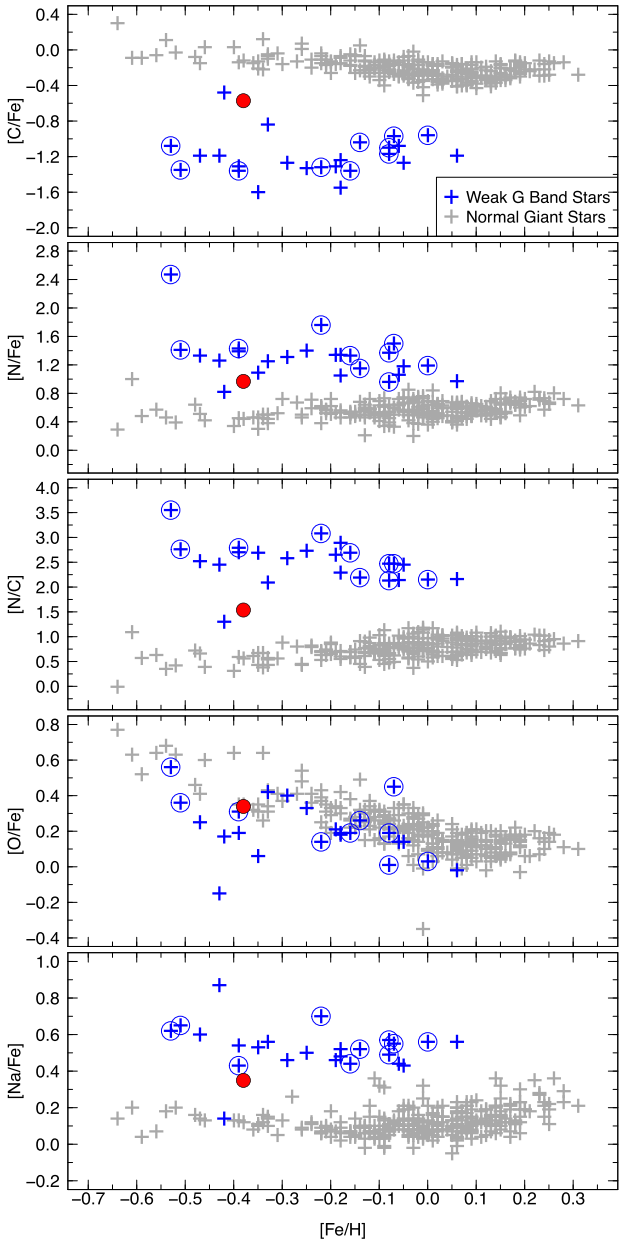

Figure 3. Abundance ratios for normal giant stars (Luck & Heiter 2007) and WGB stars (Adamczak & Lambert 2013). The blue circles were added for WGBs with log ε(Li) ≥ 1.50.

3 DISCUSSION

3.1 Lithium

A remarkable dilution of lithium occurs during the first ascent to the RGB stage, due to the development of an extensive convective envelope. It is estimated that objects with a high amount of Li in their atmospheres (log ε(Li) ≥ 1.5; the Li-rich giants) consist of only 1 per cent–2 per cent of the RGB stars (Wallerstein & Sneden 1982; Smiljanic et al. 2018; Gao et al. 2022, Cai et al. 2022 among others). In this context, we have shown in Fig. 3 abundance ratios for normal giants (grey; Luck & Heiter 2007) and WGB stars (blue; Adamczak & Lambert 2013) for comparison purposes. The Li-rich WGB giants (log ε(Li) ≥ 1.50) are marked with blue circles. For a discussion of chemical peculiarities of WGBs comparing to the

normal RGB stars, we analysed abundances of the Li, C, N, O, and Na. This set of these abundances help us to distinguish these two samples of giant stars. Also, it is important to clarify the two samples represented in Fig. 3: Luck & Heiter's sample is mainly composed of low-mass stars ($\langle M \rangle = 1.57 \pm 0.41\,M_{\odot}$) and some of them may suffer from Kraft Break (Kraft 1966; Kraft 1967) in the main sequence stage, i.e. these lower mass stars tend to be slow rotators. On the other hand, as we said before, the WGBs found in the literature are often intermediate-mass objects. However, when we look exclusively at the WGB stars the high rotation incidence appears not uncommon: 2 objects investigated by Palacios et al. (2016) present $v \sin i \geq 10\,\mathrm{km\,s^{-1}}$ (HD 67728 and HD 165462), which represents ∼10 per cent of their sample.

A possible connection between high $v \sin i$ and Li enrichment is frequently evoked in the context of Li-rich giants: this class is composed of low-mass giants generally in the RGB bump or RC phase and, less commonly, in the early-AGB (for instance, Reddy & Lambert 2016; Smiljanic et al. 2018; Holanda, Drake & Pereira 2020a). However, the high lithium abundance is not common to all WGBs reported in the literature; these classes may be 'well-separated' in the H–R diagram as Palacios et al. (2012) pointed out. Furthermore, recently Deepak, Lambert & Reddy (2020) found an interesting result about the most Li-rich giants: carbon is slightly underabundant relative to normal giants among the super Li-rich giants ($\log \varepsilon(\mathrm{Li}) \geq 3.2$). They suggest that the creation of super Li-rich giants may occur with additional CN-cycle conversion of C to N – their results are based on the GALAH data survey (De Silva et al. 2015; Buder et al. 2018). Looking to HD 16424, we see a low-mass object with Li abundance close to the limit of 'super' abundance and a carbon deficiency compared to these most Li-enriched giants and also to the WGB giants (more massive objects), which suggests an 'intermediate' effect caused by CN-cycle in low-mass stars.

Palacios et al. (2016) reported an incidence of ∼39 per cent of lithium-enriched WGB stars – here we consider $\log \varepsilon(\mathrm{Li}) \geq 1.5$ dex as the criterion to identify Li-rich giants, while they considered $\log \varepsilon(\mathrm{Li}) \geq 1.4$ dex. Adamczak & Lambert's sample contains 10 Li-rich objects, i.e. ∼42 per cent of their sample. So, lithium enrichment is not uncommon in WGB stars. Nevertheless, the high abundance of lithium-7 (so far called 'lithium abundance') should not be seen as a unique argument, but in parallel with other chemical tracers that may provide a clue to the mechanism of the formation of peculiar stars.

3.2 CNO and the isotopic ratio

As common characteristics with the WGB sample, HD 16424 star presents a high [N/C] ratio and low $^{13}C/^{13}C$: mainly, its [C/Fe] and [N/Fe] ratios are similar to those of a WGB stars, for example, HD 120171, analysed by Adamczak & Lambert (2013). Also, it is possible to see that these two objects have an intermediate [N/C] ratio values between extreme WGB and normal giants, as suggested by the authors of the quoted article for HD 120171.

At the early stages of the RGB phase the first dredge-up acts and mix into the envelope the partial product of H burning, i.e. ^{4}He and the products of CNO cycles: a decrease in ^{12}C (∼30 per cent) and an increase in ^{14}N and ^{13}C amount (Karakas & Lattanzio 2014). Another element such as Na is affected but with strong dependence in a mass interval (see Section 3.3). The [C/Fe] value expected for a normal giant star with HD 16424's metallicity is about 0.0 (Luck & Heiter 2007), but HD 16424 presents a significant C underabundance: this may be interpreted as an intermediate value, since the 'extreme' WGBs are even poorer in carbon. Additionally, the $^{12}C/^{13}C$ ratio almost reaches the CN-cycle equilibrium value (≈ 3.6).

The nitrogen overabundance suggests the action of the ON-cycle: similar to the carbon abundance, HD 16424 presents an intermediate value (and close to HD 120171). But, it is important to point out that Li atoms are destroyed by proton-capture at 2×10^{6} K, which is low for the CNO cycles to operate – so the beryllium transport mechanism should occur to create a Li-rich star. To justify the WGB phenomenon, Adamczak & Lambert (2013) evoked rapidly rotating main-sequence stars as progenitors: this scenario can provide rotationally induced mixing as a mechanism to conduct CN-cycled material to the stellar atmosphere. Of course, it is a speculative suggestion with many questions to clarify since the WGB phenomenon presents a very low incidence in post-main-sequence stars.

On other hand, Bond (2019) shows that WGBs lie at systematically larger distances from the Galactic plane than normal giants: he argues in favour of binary mass transfer and mergers as a clue to the formation of WGB stars. HD 16424 has $|Z| = 0.63$ kpc, which may agree with Bond's hypothesis. For this discussion, the author takes into account the results by Izzard et al. (2018) who studied binary stars in the Galactic thick disc, and suggests a channel for the formation of carbon-poor and nitrogen-rich stars via mass transfer in low-mass Algol systems. Concerning to HD 16424 population, this star presents spacial velocities similar to a thin disc star (Table 1) and no significant difference in RV value compared to GAIA's results, which may sound like characteristics contrary to the hypothesis raised by Izzard et al. (2018). Curiously, Zhang et al. (2020) used a similar scenario to explain the formation of Li-rich and C-rich giants without enrichment of *s*-process elements, where this time a merger of a helium-core white dwarf with an RGB star as a causer event, i.e. a post-merge object with opposite WGB characteristics – TYC 8327-1678-1 is an example of Li-rich giant with slight C enrichment studied by Holanda, Drake & Pereira (2020b).

3.3 Sodium and heavy elements

Increase in sodium abundance is expected mainly for RGB intermediate-mass stars (Smiljanic et al. 2009, 2016; Lagarde et al. 2012, among others). Thus, the sodium abundance found in HD 16424's atmosphere is considered slightly high for a normal giant star with similar mass and metallicity – see Fig. 3 to do this comparison. With the exception of HD 120171, the stars analysed by Adamczak & Lambert (2013) present remarkable sodium enrichment.

AGB stars with mass $\gtrsim 4.0\,M_{\odot}$ can activate the CNO cycle on the base of the convective envelope, the hot bottom burning (HBB), and convert the freshly synthesized ^{12}C into ^{14}N and ^{13}C (Boothroyd & Sackmann 1999). In addition, the Ne-Na and Mg-Al chains may also operate to produce ^{23}Na and Al atoms at the bottom convective envelope temperatures $>70 \times 10^{6}$ K (Kobayashi, Karakas & Umeda 2011; Karakas & Lattanzio 2014; Abia, Straniero & Ventura 2017). Moreover, HBB can provide lithium-7 nucleosynthesis through the Cameron–Fowler mechanism (Cameron & Fowler 1971), as reported for luminous AGB stars with intermediate-mass in the Magellanic Clouds and Milky Way (Smith & Lambert 1990; Plez, Smith & Lambert 1993; García-Hernández et al. 2007). In other words, the chemistry provided by a thermally pulsing AGB star could explain partially the abundances derived here. For heavy elements produced via a slow neutron capture process (Y, Zr, and La) we did not find any enrichment ($[s/\mathrm{Fe}] = -0.02$), which help us to disregard the scenario of contamination via an evolved AGB companion. That said,

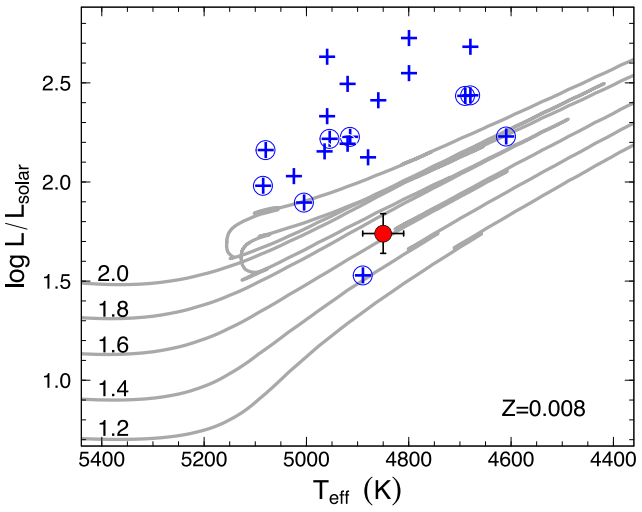

Figure 4. HD 16424 in the temperature–luminosity diagram based on derived spectroscopic parameters. Evolutionary tracks are from Bressan et al. (2012). The sample analysed by Adamczak & Lambert (2013) is represented in blue colour.

the uncommon abundances observed in HD 16424's atmosphere are exclusively those typically discussed in the WGB star context (C, N, Li, Na, and $^{12}C/^{13}C$).

3.4 Evolutionary status

Determining the evolutionary status of WGBs may be fundamental to understanding the mechanism responsible for their peculiarities. The HD 16424 star is a low mass object (1.61 $M_{\odot}$; Fig. 4): this result is based on $T_{\rm eff}$, log g, and parallax via PARAM. Temperature and spectroscopic gravity are in excellent concordance with photometric value ($\Delta T_{\rm eff} = -28$ K and $\Delta \log g = +0.01$) and the parallax measurement presents a small uncertainty, about ∼3 per cent of the total value, which gives reliability to the results presented here. So, the low mass of HD 16424 is in contrast with most WGB stars analysed in the literature (e.g. Adamczak & Lambert 2013; Palacios et al. 2016; Bond 2019). The star HD 16424 is at the RGB stage in the Hertzsprung–Russel diagram present in Fig. 4, but there is an important caveat: it is an ambiguous region if we consider the uncertainties (it is close to RC).

Still, HD 16424 is an evolved object that is beyond the RGB base or the red part of the Hertzsprung Gap (see Fig. 4), but if we consider uncertainties in effective temperature and luminosity, its location is ambiguous: low-mass RGB stars are objects with helium degenerated core and burning hydrogen in a thin shell surrounding this one, while low-mass RC stars are burning helium in the core and experimenting helium flash. The solution to this problem lies in the analysis of asteroseismic parameters as has been explored in studies of lithium-rich giants (e.g. Singh et al. 2019; Deepak & Lambert 2021). Due to the unavailability of this data, we suggest based on the precise atmospheric parameter and luminosity values that the HD 16424 star is into the RGB stage.

4 CONCLUSIONS

Based on high-quality data, we analysed the chemical abundances of the puzzling HD 16424 star. We have taken from the literature astrometric and photometric data to provide more parameters to make a discussion about the possible origin of an atypical amount of lithium and ^{13}C. Below are some important results:

(i) The spectroscopic and photometric stellar parameters of HD 16424 indicate that it is a low mass star (1.61 $M_{\odot}$) located in an dubious region of the H–R diagram – between the ascension to RGB (luminosity bump) and RC stage. To investigate its status, we used evolutionary tracks by Bressan et al. (2012) for subsolar metallicity ($Z = 0.008$). But, an assertive conclusion about this evolutionary stage would be possible through derived parameters from asteroseismic data.

(ii) The carbon isotopic ratio found by us is surprisingly low, which can be associated with a mechanism of lithium enrichment. Alternatively, $^{12}C/^{13}C = 4.0$ suggests a deep mixing or accretion of material rich in ^{13}C – a companion in an advanced evolutionary stage? It is well-known that AGB stars can produce large amounts of ^{13}C, but the lack of divergence in radial velocities (compared to GAIA value) does not confirm a binary nature of this star.

(iii) We did not find any evidence of chemical contamination by an evolved AGB companion: the set of s-process elements presents an abundance typical of red giants. This result indicates that HD 16424 origin must be sought in a single-star evolution scenario, as verify Tomkin, Sneden & Cottrell (1984) for the WGB phenomenon. Furthermore, our result for metallicity is subsolar and matches with the range discussed by Adamczak & Lambert (2013) and Bond (2019). Thus, it seems that WGB stars are objects formed in low metallicity environment: is this a requirement to form a WGB star? Large spectroscopic surveys could shed light on this issue.

The results found for HD 16424 show that an explanation for the origin of the so-called weak *G*-band stars depends on many parameters and we can not limit their formation from intermediate-mass progenitors, although most of these stars have intermediate masses as has been widely reported in the literature.

ACKNOWLEDGEMENTS

NH thanks the Conselho Nacional de Desenvolvimento Científico e Tecnológico (CNPq) for funding support (302834/2021-4). NAD acknowledges Fundação de Amparo à Pesquisa do Estado do Rio de Janeiro (FAPERJ), for grant E-26/203.847/2022. We greatly appreciate the anonymous referee for the thorough reading and suggestions that helped us to improve the manuscript. The use of the SIMBAD, VizieR, and VALD database is acknowledged.

DATA AVAILABILITY

The spectroscopic data that support the findings of this study are available from the corresponding author, NH, upon reasonable request.

REFERENCES

Abia C., Straniero O., Ventura P., 2017, Mem. Soc. Astron. Ital., 88, 360
Adamczak J., Lambert D. L., 2013, ApJ, 765, 155
Alonso A., Arribas S., Martínez-Roger C., 1999, A&AS, 140, 261
Ammons S. M., Robinson S. E., Strader J., Laughlin G., Fischer D., Wolf A., 2006, ApJ, 638, 1004
Antipova L. I., Boyarchuk A. A., Pakhomov Y. V., Yushkin M. V., 2005, Astron. Rep., 49, 535
Asplund M., Grevesse N., Sauval A. J., Scott P., 2009, ARA&A, 47, 481
Bai Y., Liu J., Bai Z., Wang S., Fan D., 2019, AJ, 158, 93
Bessell M. S., Castelli F., Plez B., 1998, A&A, 333, 231

Bidelman W. P., 1951, ApJ, 113, 304
Bidelman W. P., MacConnell D. J., 1973, AJ, 78, 687
Bond H. E., 2019, ApJ, 887, 12
Boothroyd A. I., Sackmann I. J., 1999, ApJ, 510, 232
Bressan A., Marigo P., Girardi L., Salasnich B., Dal Cero C., Rubele S., Nanni A., 2012, MNRAS, 427, 127
Buder S. et al., 2018, MNRAS, 478, 4513
Cai B., Kong X., Shi J., Gao Q., Bu Y., Yi Z., 2022, preprint (arXiv:2211.06608)
Cameron A. G. W., Fowler W. A., 1971, ApJ, 164, 111
Coşkunoğlu B. et al., 2011, MNRAS, 412, 1237
Cutri R. M. et al., 2013, VizieR Online Data Catalog, II/328
da Silva L. et al., 2006, A&A, 458, 609
De Silva G. M. et al., 2015, MNRAS, 449, 2604
Deepak , Lambert D. L., Reddy B. E., 2020, MNRAS, 494, 1348
Deepak, Lambert D. L., 2021, MNRAS, 505, 642
Drake N. A., Pereira C. B., 2008, AJ, 135, 1070
Fekel F. C., 1997, PASP, 109, 514
Gaia Collaboration 2018, A&A, 616, A1 (G2018)
Gao J., Zhu C., Yu J., Liu H., Lu X., Shi J., Lü G., 2022, preprint (arXiv:2210.13152)
García-Hernández D. A., García-Lario P., Plez B., Manchado A., D'Antona F., Lub J., Habing H., 2007, A&A, 462, 711
Gontcharov G., 2008, Astronomy Letters, 34, 785
Gray D. F., 1989, ApJ, 347, 1021
Hobbs L. M., Thorburn J. A., Rebull L. M., 1999, ApJ, 523, 797
Høg E. et al., 2000, A&A, 355, L27 (H2000)
Holanda N., Drake N. A., Corradi W. J. B., Ferreira F. A., Maia F., Magrini L., da Silva J. R. P., Pereira C. B., 2021, MNRAS, 508, 5786
Holanda N., Drake N. A., Pereira C. B., 2020a, AJ, 159, 9
Holanda N., Drake N. A., Pereira C. B., 2020b, MNRAS, 498, 77
Holanda N., Ramos A. A., Peña Suárez V. J., Martinez C. F., Pereira C. B., 2022, MNRAS, 516, 4484
Houk N., Smith-Moore M., 1988, Michigan Catalogue of Two-dimensional Spectral Types for the HD Stars. Volume 4, Declinations −26.0 to −12.0 deg. Department of Astronomy, University of Michigan, Ann Arbor, (H1988)
Izzard R. G., Preece H., Jofre P., Halabi G. M., Masseron T., Tout C. A., 2018, MNRAS, 473, 2984
Johnson D. R. H., Soderblom D. R., 1987, AJ, 93, 864
Karakas A. I., Lattanzio J. C., 2014, Publ. Astron. Soc. Aust., 31, e030
Kaufer A., Stahl O., Tubbesing S., Nørregaard P., Avila G., Francois P., Pasquini L., Pizzella A., 1999, The Messenger, 95, 8
Kobayashi C., Karakas A. I., Umeda H., 2011, MNRAS, 414, 3231
Kraft R. P., 1966, ApJ, 144, 1008
Kraft R. P., 1967, ApJ, 150, 551
Kupka F., Piskunov N., Ryabchikova T. A., Stempels H. C., Weiss W. W., 1999, A&AS, 138, 119
Kurucz R., 1993, ATLAS9 Stellar Atmosphere Programs and 2 km/s grid. Kurucz CD-ROM No. 13. Smithsonian Astrophysical Observatory, Cambridge, p. 13
Lagarde N., Decressin T., Charbonnel C., Eggenberger P., Ekström S., Palacios A., 2012, A&A, 543, A108
Lambert D. L., Heath J. E., Lemke M., Drake J., 1996, ApJS, 103, 183
Lambert D. L., Sawyer S. R., 1984, ApJ, 283, 192
Lawler J. E., Bonvallet G., Sneden C., 2001, ApJ, 556, 452
Lind K., Asplund M., Barklem P. S., 2009, A&A, 503, 541
Lind K., Asplund M., Barklem P. S., Belyaev A. K., 2011, A&A, 528, A103
Luck R. E., Heiter U., 2007, AJ, 133, 2464
McDonald I., Zijlstra A. A., Watson R. A., 2017, MNRAS, 471, 770
Palacios A., Jasniewicz G., Masseron T., Thévenin F., Itam-Pasquet J., Parthasarathy M., 2016, A&A, 587, A42
Palacios A., Parthasarathy M., Bharat Kumar Y., Jasniewicz G., 2012, A&A, 538, A68
Pickles A., Depagne É., 2010, PASP, 122, 1437 (PD2010)
Plez B., Smith V. V., Lambert D. L., 1993, ApJ, 418, 812
Ramírez I., Allende Prieto C., Lambert D. L., 2007, A&A, 465, 271
Rao N. K., 1978, MNRAS, 185, 585
Reddy A. B. S., Lambert D. L., 2016, A&A, 589, A57
Reddy B. E., Tomkin J., Lambert D. L., Allende Prieto C., 2003, MNRAS, 340, 304
Roriz M. P., Lugaro M., Pereira C. B., Sneden C., Junqueira S., Karakas A. I., Drake N. A., 2021, MNRAS, 507, 1956
Singh R., Reddy B. E., Bharat Kumar Y., Antia H. M., 2019, ApJ, 878, L21
Smiljanic R. et al., 2016, A&A, 589, A115
Smiljanic R. et al., 2018, A&A, 617, A4
Smiljanic R., Gauderon R., North P., Barbuy B., Charbonnel C., Mowlavi N., 2009, A&A, 502, 267
Smith V. V., Cunha K., Jorissen A., Boffin H. M. J., 1996, A&A, 315, 179
Smith V. V., Lambert D. L., 1990, ApJS, 72, 387
Smith V. V., Lambert D. L., Nissen P. E., 1998, ApJ, 506, 405
Sneden C. A., 1973, PhD thesis, The University of Texas at Austin
Sneden C., McWilliam A., Preston G. W., Cowan J. J., Burris D. L., Armosky B. J., 1996, ApJ, 467, 819
Tody D., 1986, in Crawford D. L., ed., Proc. SPIE Conf. Ser. Vol. 627, Instrumentation in Astronomy VI. SPIE, Bellingham, p. 733
Tomkin J., Sneden C., Cottrell P. L., 1984, PASP, 96, 609
Tonry J. L. et al., 2018, ApJ, 867, 105
Tsvetkova S., Petit P., Konstantinova-Antova R., Aurière M., Wade G. A., Palacios A., Charbonnel C., Drake N. A., 2017, A&A, 599, A72
Van Winckel H., Reyniers M., 2000, A&A, 354, 135
Wallerstein G., Sneden C., 1982, ApJ, 255, 577
Wiese W. L., Smith M. W., Miles B. M., 1969, Atomic Transition Probabilities. Vol. 2: Sodium through Calcium. A Critical Data Compilation. NSRDS-NBS, Washington, DC
Zhang X., Jeffery C. S., Li Y., Bi S., 2020, ApJ, 889, 33

This paper has been typeset from a TEX/LATEX file prepared by the author.